




A new MgB₂ bulk ring fabrication technique for use in magnetic shielding or bench-top NMR systems

D A Moseley^{1,2,*} , D P Wilkinson³, T Mousavi⁴, A R Dennis¹, S Speller⁴ 
and J H Durrell¹ 

¹ Department of Engineering, Cambridge University, Trumpington Road, Cambridge CB2 1PZ, United Kingdom

² Robinson Research Institute, Victoria University of Wellington, 69 Gracefield Road, Lower Hutt 5010, New Zealand

³ Ludwig-Maximilians-Universität München, Geschwister-Scholl-Platz 1, 80539 München, Germany

⁴ Department of Materials, Oxford University, Banbury Road, Oxford OX2 6HT, United Kingdom

E-mail: dominic.moseley@vuw.ac.nz

Received 31 March 2022, revised 24 May 2022

Accepted for publication 1 June 2022

Published 30 June 2022



Abstract

We report a new methodology in bulk MgB₂ ring production for use in small-scale magnetic shielding or bench-top nuclear magnetic resonance systems. This process is a modified field-assisted sintering technique (mFAST) which enables direct formation of the rings without the need for machining or additives into the precursor powder. The shielding and trapped field capabilities of three mFAST MgB₂ rings were determined using zero-field- and field-cooled magnetic experiments. Individual bulks trap magnetic fields up to 1.24 T at 20 K comparable to the highest published data for a ring sample. It is anticipated that for many applications, multiple rings will be stacked to form the required experimental structure. We find, for the three ring stack, a trapped field of 2.04 T and a maximum shielded field of 1.74 T at 20 K. The major factor limiting performance at low temperatures are flux jumps which cause rapid loss of the trapped field or shielding capability. Preliminary studies of magnetic field ramp rate dependence on flux jumps were conducted illustrating that even at very slow ramp rates (0.007 T min⁻¹) they remain a significant issue. Despite this concern, we conclude that mFAST represents an exciting new fabrication methodology for bulk MgB₂ rings.

Supplementary material for this article is available [online](#)

Keywords: MgB₂, magnetic shielding, NMR, bulk superconductors

(Some figures may appear in colour only in the online journal)

* Author to whom any correspondence should be addressed.



Original content from this work may be used under the terms of the [Creative Commons Attribution 4.0 licence](#). Any further distribution of this work must maintain attribution to the author(s) and the title of the work, journal citation and DOI.

1. Introduction

Large-scale bulk samples are gaining traction as a new approach for the implementation of high temperature superconductors (HTSs). Two applications where bulks can play a significant role are magnetic shielding and bench-top nuclear magnetic resonance (NMR) [1, 2]. In these applications, the ideal bulk topology is a ring as it provides direct access to the geometric centre of the sample. However, accurate characterisation for each application requires slightly different techniques. In magnetic shielding, superconducting screening currents within the bulk act to magnetically protect an internal volume. Therefore, this behaviour is best characterised by measuring the magnetic field response at the bulk centre during the initial up-sweep of zero-field-cooled (ZFC) magnetisation. In contrast, for bulk-based NMR, it is the trapped magnetic field at zero applied field after field-cooled (FC) magnetisations (B_{FC}) that is the figure of merit. In this case, the B_{FC} works as a quasi-permanent magnet which can be used as the dc background magnetic field for NMR. For NMR, increasing the spatial homogeneity and temporal stability of B_{FC} is also essential.

Due to the origin of the magnetic shielding and B_{FC} , bulks in these applications effectively act as passive components without the need for external control. This potentially makes the systems simpler and smaller than conventional superconducting electromagnets. The lack of an external control structure means that superconducting joints can be removed from the system design. It is well established that HTS joints are a significant issue [3] which are particularly pertinent for NMR systems. In NMR, the magnetic field decay must be in the range of parts per billion for real-world systems [4] which should be readily achievable with bulk superconductors [1, 5].

To date, most bulk superconductor research has focussed on (RE)–Ba–Cu–O [(RE)BCO] cuprates due to the potential of trapped fields up to 17.6 T [6–8]. However, (RE)BCO bulks are difficult to manufacture, brittle and relatively dense (6.4 g cm^{-3}) [9, 10]. MgB_2 is considered a promising alternative for specific applications due to its range of physical properties. Not only is MgB_2 light (2.4 g cm^{-3}) and mechanically robust [1], but the base materials are cheap. While the critical superconducting temperature ($\sim 39 \text{ K}$) is lower than (RE)BCO it still lies within the capability of single-stage cryocoolers making system design uncomplicated. However, the main trade-off is the reduction in absolute performance. To date, a maximum B_{FC} of 4.6 T in pure MgB_2 has been achieved [11]. Therefore, MgB_2 applications will be limited to low field applications particularly where weight is a significant issue [12].

In addition to these physical advantages, MgB_2 has a unique superconducting property which makes it ideal for bulks. Due to MgB_2 large coherence lengths (in the *ab*-plane: $39 \pm 11 \text{ nm}$, and $35 \pm 10 \text{ nm}$ in the *c*-plane [13]) even polycrystalline samples can act as a continuous bulk superconductor. Not only does this make bulk synthesis relatively straightforward but it also eradicates the growth sector boundary related inhomogeneous field distribution observed in (RE)BCO bulks [9].

To date, two distinct synthesis methodologies are used for MgB_2 bulks: field-assisted sintering technique (FAST) [14, 15] and reactive liquid Mg infiltration [16]. While the size of infiltration growth samples is only limited by the reaction chamber, FAST samples have been shown to produce the highest J_C and therefore have the potential to shield or trap greater fields [2]. However generating large ring bulks with FAST is not trivial. FAST requires high temperature and pressure which places the bulk under significant stresses during the manufacturing process [17]. In the existing literature, FAST has only been used to directly fabricate disks or solid cylinders of MgB_2 which cannot be simply used for magnetic shielding or NMR systems. However, machining is complicated by the mechanical strength of pure MgB_2 which can lead to damage of the bulk structure during this process. To counteract this, Gozzelino *et al* [15] have developed a technique where pure MgB_2 powder is mixed with hexagonal boron nitride before the FAST process. This reduces the strength making machining possible but potentially reducing the superconducting properties making this process non-ideal. We note that Naito *et al* [18] also successfully machined a ring of comparable size from a hot isostatic pressed bulk although the reproducibility of this process was not discussed. In this work, we outline a modified FAST (mFAST) process which achieves the goal of direct fabrication of MgB_2 bulk rings without machining or precursor additives and investigate the superconducting properties using magnetisation experiments.

2. Experimental procedure

2.1. Ring manufacturing—mFAST

A two-stage fabrication approach is necessary to generate rings using mFAST. Initially, disk samples are formed using a conventional *ex-situ* FAST approach [19]. Commercial MgB_2 powder was compressed into a graphite mould and placed into Dr Fritsch DSP507 FAST machine (<https://dr-fritsch.de/>). Through an iterative study, the optimum conditions for generating dense bulks was established. Following our previous study [14], we find a sintering time of 5 min with a pressure of 50 MPa and temperature of 1150°C produced samples with the highest trapped field and a measured density of 96%. These re-usable disks play an essential role in the ring formation by operating as the internal structures generating the inner ring radius.

To generate ring samples, a bespoke mould structure was developed consisting of graphite outer former, ring stamp and half-shells with a unique internal pin structure, as shown in figures 1(a) and (b). The internal pin structure must be formed using the pre-pressed MgB_2 bulk disk sandwiched between two graphite pins, as displayed in figure 1(c). All surfaces were covered with graphite paper throughout this process. This construction ensures that the thermal contraction rates of the formed ring and internal pin structure are matched, significantly minimising temperature induced stresses. In combination with close control of the cooling profile, this experimental structure maintains the structural stability of the ring throughout the mFAST procedure. If a uniform graphite pin is utilised,

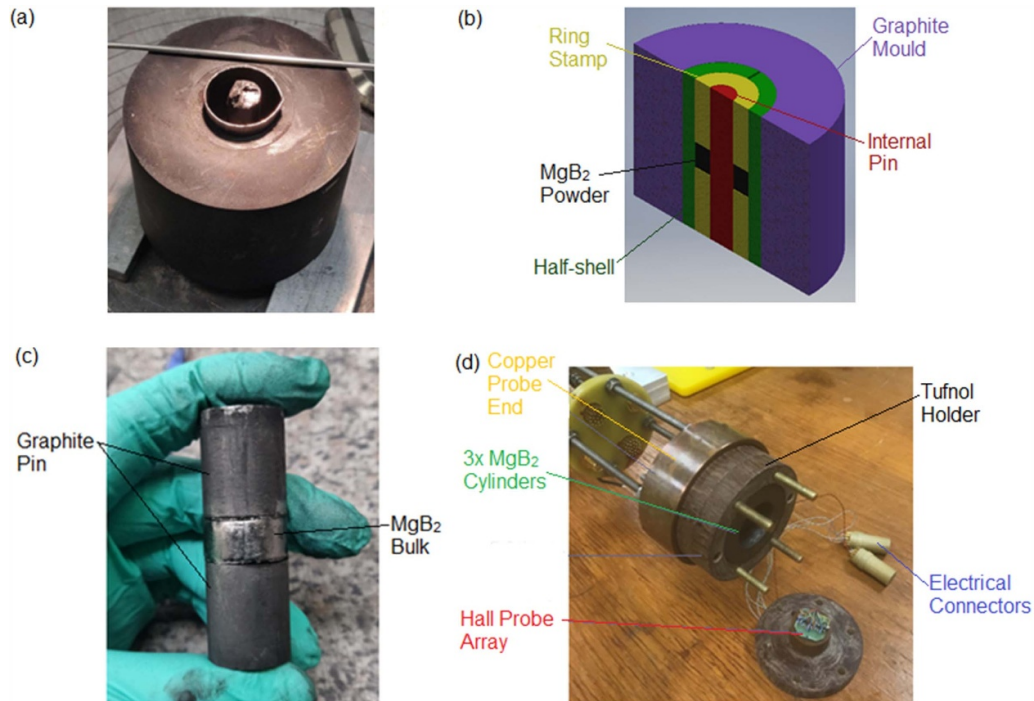


Figure 1. (a) Photograph of bespoke mould for ring manufacture. (b) Labelled cut-through schematic of mould. (c) Internal pin structure. (d) Labelled picture of ring holder.

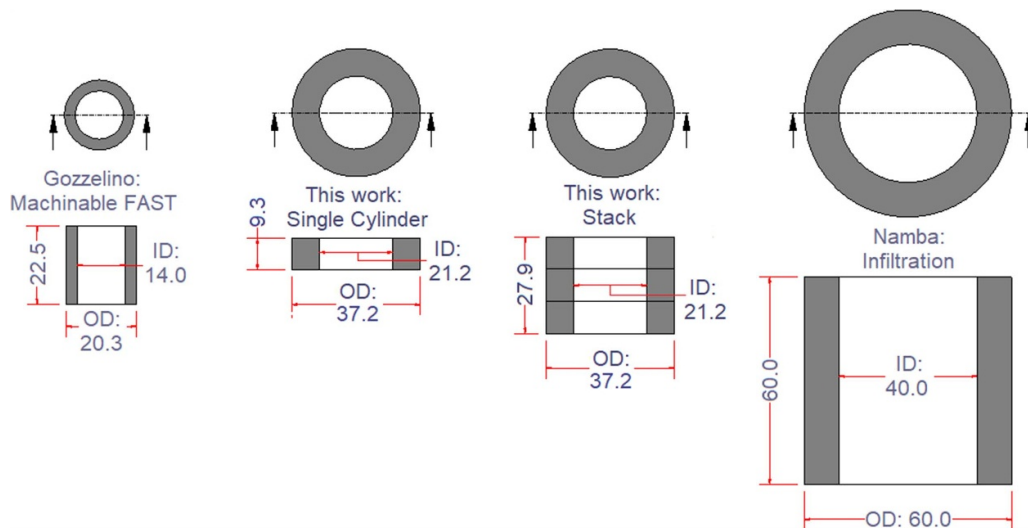


Figure 2. Comparison between literature samples and the rings used in this work, to scale.

the mFAST methodology did not reproducibly generate bulk rings of the size displayed in figure 2. Instead, after the sintering process, the rings were found to be fractured.

This process generated three MgB_2 rings with dimensions of 37 mm outer diameter, 21 mm inner diameter and 9.3 mm thickness. In figure 2, the samples considered in this work are displayed to scale with existing literature MgB_2 rings. The physical size of the samples lie in between the existing machinable FAST samples discussed by Gozzelino *et al* [2, 15] and the larger Namba *et al* [20] samples formed by infiltration

growth. However, they are a similar size to the machined samples of Naito *et al* [18].

2.2. Microstructural characterization

X-ray diffraction (XRD) measurements were performed using a PANalytical Empyrean diffractometer with $\text{CuK}\alpha$ radiation ($\lambda = 0.154$ nm) at 40 kV and 40 mA. The weight fraction of the different phases present in the samples were estimated from the XRD patterns using Rietveld refinement

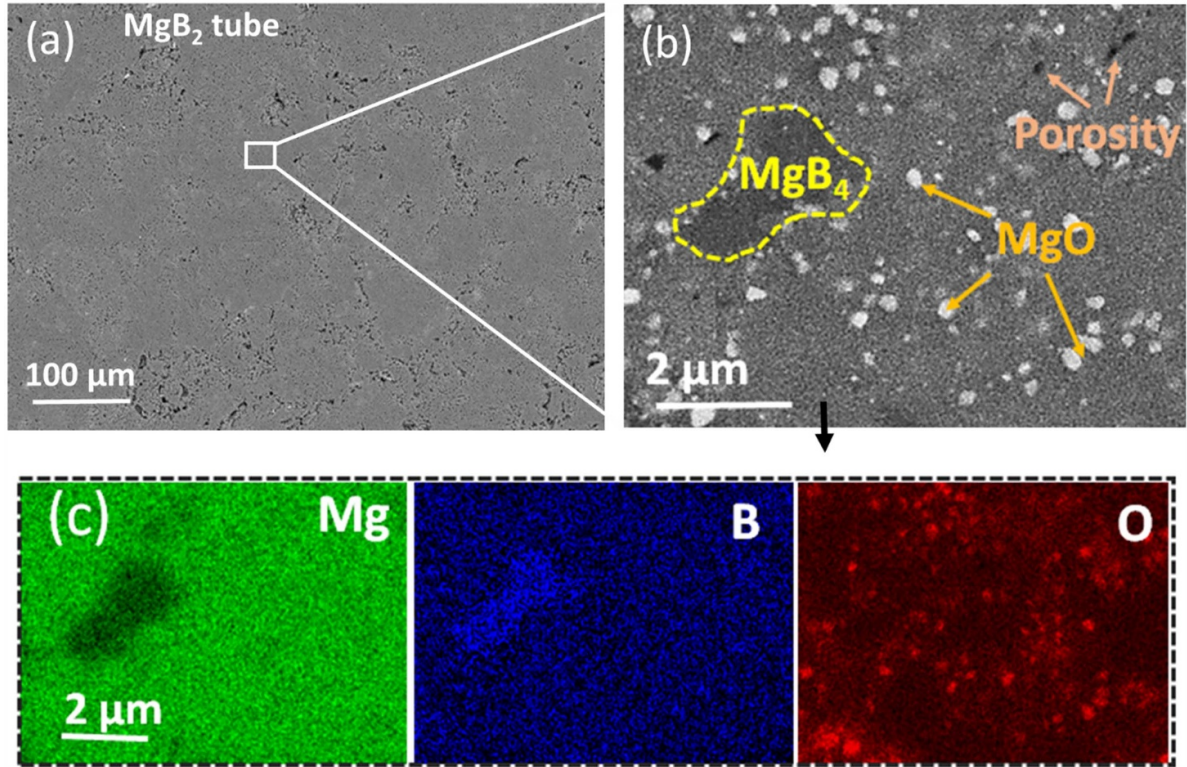


Figure 3. Scanning electron microscopy analysis of an MgB_2 ring sample. Backscattered electron images at (a) low magnification and (b) high magnification showing the homogeneity, porosity, and distribution of impurity phases in the sample. (c) Energy dispersive x-ray spectroscopy maps showing distribution of elements in the sample.

(PANalytical HighScore Plus software). Scanning electron microscopy (SEM) analysis was carried out using a Zeiss Merlin SEM with an Oxford Instruments 150 mm² XMax EDX detector.

2.3. Magnetisation experiments

Magnetic measurements were performed using a 12 T large bore magnet system (ICEoxford, UK). The samples were measured as individual rings and as a stack of three rings. In both cases, the rings were coated with a thin layer of Apiezon-N cryogenic grease (M&I Materials Ltd) and inserted into a tufnol holder. The structure was then clamped onto a copper mounting plate, as shown in figure 1(d). The temperature was measured using an in-built Cernox thermometer embedded in the copper mounting plate. The entire measurement apparatus was installed in a helium-flow variable temperature insert allowing precise temperature control. An experimentally calibrated hall sensor (Lakeshore HGT-2101) was positioned at the ring or stack centre aligned to measure the field along the longitudinal axis. Both the FC and ZFC behaviours were measured at a range of temperatures (5 K, 10 K, 15 K, 20 K, 25 K, 30 K) with two magnetic field ramp rates (0.025 T min⁻¹ and 0.007 T min⁻¹).

The magnetic shielding is characterised by the shielding ratio (S_R) [2] during the initial upward positive field sweep:

$$S_R = \frac{B_Z(T)}{\mu_0 H(T)}$$

where $\mu_0 H(T)$ is the applied magnetic field. We assign $S_R < 0.01$ (S_R (99%)) as representing complete shielding of the external magnetic field.

3. Results

Figure 3 shows the microstructure of a typical ring bulk sample. At low magnification, the sample shows a well-connected microstructure containing a small volume fraction of pores (black regions) illustrating the high quality of the produced samples. At higher magnification (figure 3(b)) four different contrast levels can be observed. These correspond to the solid phases of MgB_2 (light grey), MgB_4 (dark grey) and MgO (white), and porosity (black). This phase assignment has been confirmed by energy dispersive X-ray elemental maps presented in figure 3(c). This data shows that the MgB_2 ring consists of a connected matrix of MgB_2 phase with very fine round MgO particles (<1 μm) and individual larger particles of MgB_4 (2–10 μm) randomly distributed over the matrix. The sample shows a fairly dense microstructure with small individual pores which are not expected to interrupt a continuous path for supercurrent. The volume fraction of MgO in the sample was estimated by image contrast analysis to be 4.3 vol.% (~6.5 wt.%) consistent with 6 wt.% calculated by XRD and with existing non-ring FAST samples [14]. Further details can be found in the related supplementary material.

In figure 4(a), the $B_Z(T)$ response for the initial positive magnetic field down sweep (5 T–0 T) after FC at 10 K, 20 K and 30 K for the stack is displayed. The 20 K data for a single

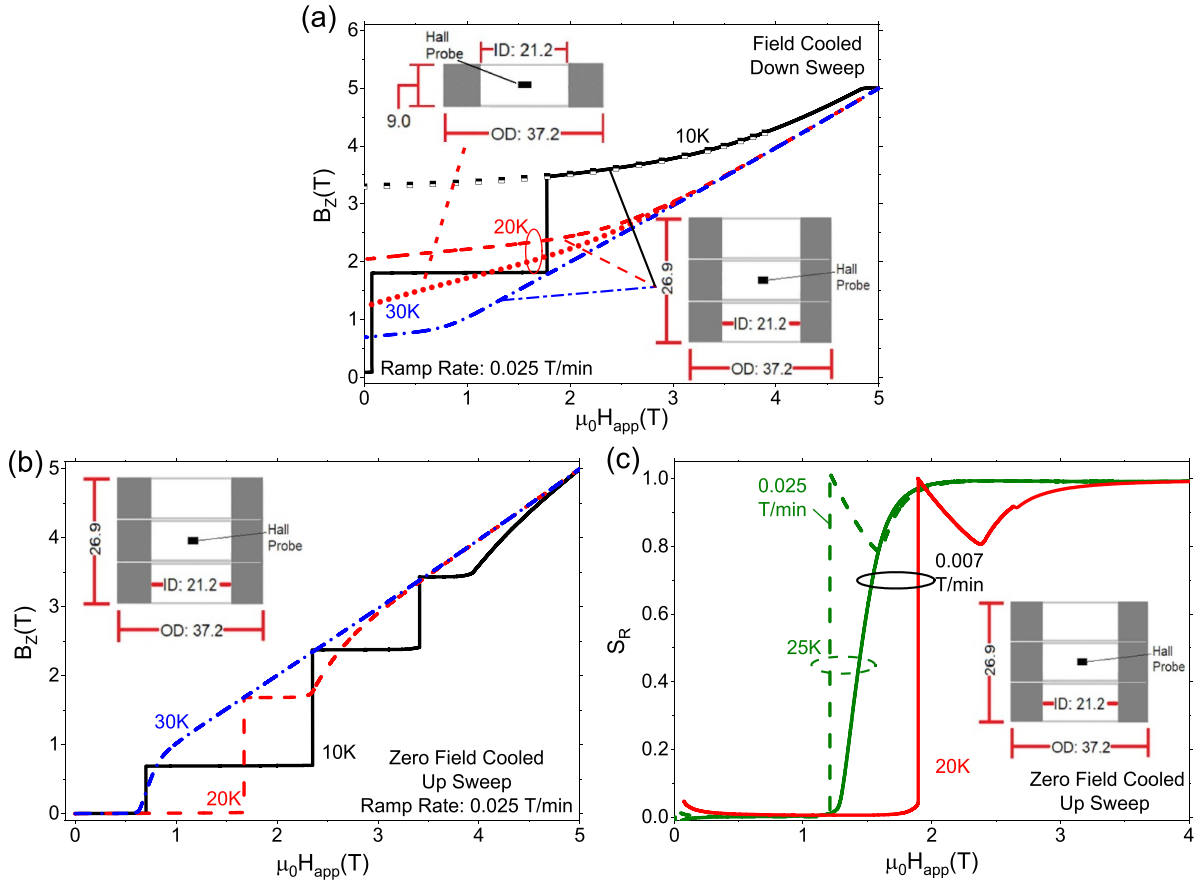


Figure 4. (a) Field-cooled positive field down sweep internal magnetic field response for three MgB₂ stack using 0.025 T min⁻¹ ramp rate at 10 K, 20 K and 30 K and 20 K for single MgB₂ ring (red circles). Black square symbols represents extrapolated data for 10 K MgB₂ stack FC response. (b) Zero-field cooled positive up sweep internal magnetic field response for three MgB₂ stack using 0.025 T min⁻¹ ramp rate at 10 K, 20 K and 30 K. (c) S_R of stack at 20 K and 25 K at 0.025 T min⁻¹ and 0.007 T min⁻¹.

ring is shown for comparison. Firstly, the B_{FC} of the mFAST single rings is comparable to ring samples formed requiring additional machining [15, 18]. Secondly, the stacking of three bulks increases B_{FC} from 1.24 T to 2.04 T—a ~65% increase in B_{FC} . While this value is less than the infiltration growth Namba *et al* [20] sample (2.2 T at 20 K) the disparity stems from the greater physical size of the Namba sample (see figure 2). The generation of larger rings should enable larger B_{FC} to be achieved. While this data illustrates the potential of mFAST tubes further analysis exploring the uniformity of the generated magnetic field within the bore will be essential for NMR applications.

One significant issue are flux jumps which limit both the observed B_{FC} and shielding capability at temperatures below 25 K. Firstly, it should be noted that while flux jumps affect both the ZFC and FC measurements (which correlate to S_R (99%) and B_{FC} respectively), the ZFC experiments are more susceptible. To illustrate this variation, consider the dashed lines in figures 4(a) and (c) which display the 20 K response for FC and ZFC during the initial upward field ramp using a 0.025 T min⁻¹ ramp rate respectively. In the FC scenario (figure 4(a)) the stack is resilient to flux jumps. Conversely, in ZFC a flux jump is observed. Indeed, flux jumps are observed at all temperatures below 25 K in the ZFC scenario (dashed

line, figure 4(d)) while they are only observed at 15 K and below in FC. Due to flux jumps, the maximum shielded field using S_R (99%) was observed at 15 K (2.05 T). This value is comparable to the best performance in the literature [12, 15].

In figure 4(d), we consider the effect of magnetic ramp rate on the flux jump behaviour in the ZFC scenario. Lowering the ramp rate increases the flux jump resilience. For instance, with a 0.007 T min⁻¹ ramp rate at 25 K no flux jumps are observed unlike at 0.025 T min⁻¹. However, a 0.007 T min⁻¹ ramp rate remains insufficient to stop flux jumps below 25 K. This flux jump sensitivity may act as a significant limiting factor for MgB₂ based shielding applications.

In figure 5(a), the B_{FC} and S_R (99%) values at all temperature using a 0.025 T min⁻¹ magnetic ramp rate are shown. If flux jumps do not significantly alter the performance, S_R (99%) is around 85% of B_{FC} . Therefore, it is essential that the shielding ability is not directly inferred from trapped field measurements but is characterised using a ZFC methodology. To ascertain the non-flux jump performance, extrapolated values for B_{FC} were calculated using a non-linear curve fitting technique from the high field functional form. This is shown graphically by the black half squares in figure 4(a). Using this extrapolation, a B_{FC} of 3.7 T would be achieved at 5 K without flux jumps.

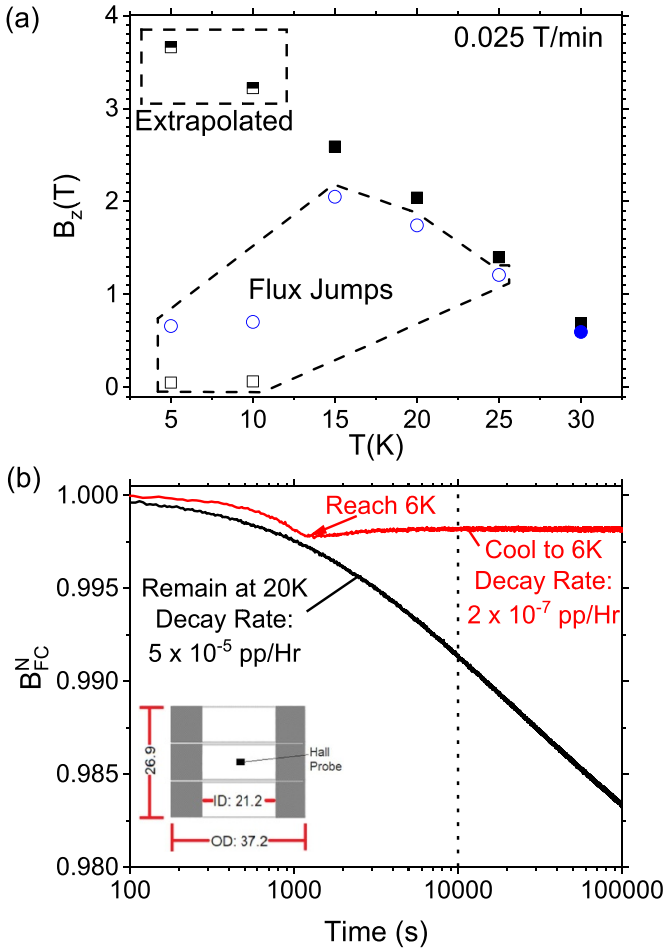


Figure 5. (a) $B_{FC}(T)$ and $S_R(99\%)$ for stack using 0.025 T min^{-1} ramp rate. Black squares (\blacksquare , \square) represent $B_{FC}(T)$ and blue circles (\bullet , \circ) represent $S_R(99\%)$. Open symbols represent response affected by flux jump. The extrapolated non-flux jump $B_{FC}(T)$ performance is shown by the half squares (\blacksquare). This is calculated by fitting an exponential function ($B_z(T) = B_{FC}(0T) + A_1 e^{-\mu_0 H_{app}/x_1}$) from 4 T to the location of the flux jump as shown by the half squares in figure 3(a). (b) Comparison of $B_{FC}(0T)$ temporal stability for stack quantified using the normalised $B_{FC}(0T)$ ($B_{FC}^N = \frac{B_{FC}(\text{Time})}{B_{FC}(0 \text{ s})}$) using two post-magnetisation temperature procedures. In one case, the stack remains at 20 K; in the other, the stack is cooled to 6 K after the magnetic down sweep. The decay rate after 10 000 s drops from 50 ppb h^{-1} in the consistent temperature procedure to 0.2 ppb h^{-1} when the stack was cooled to 6 K.

For NMR applications, it is vital that the B_{FC} temporal stability is maximised to enable long term use without continual remagnetisation. Recent work by Takahashi *et al* [1] illustrated that cooling after the magnetisation significantly improves the magnetic field persistence. However, the B_{FC} value explored in that work was substantially smaller than the absolute performance of their sample, potentially leading to an overestimation of the true persistence. Therefore, to quantify the improvement of post-magnetisation cooling, we evaluated the stability for two cases: no post-magnetisation cooling (sample remains at 20 K) and cooling of the stack to 6 K after optimal magnetisation ($B_{FC} = 2.04 \text{ T}$). We find that without cooling the field decay was 50 ppb h^{-1} , as shown in figure 5(b).

For post-magnetisation cooling, the decay rate reduces by two orders of magnitude to 0.2 ppb h^{-1} . Illustrating that excellent persistence can be achieved even near optimal B_{FC} .

4. Conclusions

We have investigated the trapped field and shielding properties of MgB_2 rings using two magnetisation procedures (FC and ZFC) as a function of temperature, applied magnetic field magnitude and ramp rate. The rings were directly formed without machining using modified FAST. In modified FAST, a unique internal pin structure, using a pre-formed MgB_2 bulk, is used to generate the internal ring radius. This process reproducibly generates ring bulks with dimensions of 37 mm outer diameter, 21 mm inner diameter and 9.3 mm thickness. The individual rings demonstrate a 20 K trapped field of 1.24 T which increases to 2.04 T for a stack of three rings at 20 K. Therefore, this new fabrication methodology demonstrates significant promise for producing high quality ring bulks with properties beyond the existing literature data.

Flux jumps play a significant role in limiting the performance of the stack. This is particularly acute in zero-field-cooling and, therefore, shielding scenarios. At temperatures below 30 K, flux jumps are observed in the ZFC data using a 0.025 T min^{-1} applied field ramp rate. In comparison, flux jumps are only observed at temperatures below 15 K in the FC data. These flux jumps limit the observed shielding field to the 2.05 T seen at 15 K. The flux jump stability can be improved using a slower ramp rate, however, the sensitivity to flux jumps must be considered a significant hindrance for magnetic shielding applications.

Finally, the stack trapped field temporal stability was explored for FC magnetisation at 20 K using two different post-magnetisation procedures. If the stack is cooled to 6 K after magnetisation, the field decay decreases to 0.2 ppb h^{-1} representing $250\times$ improvement in trapped field persistence compared to no cooling after magnetisation. Further work exploring the homogeneity of the trapped field and methodologies for the limiting the effect of flux jumps will be essential for real-world applications.

Data availability statement

The data that support the findings of this study are openly available at the following URL/DOI: [10.17863/CAM.78758](https://doi.org/10.17863/CAM.78758). The University of Cambridge would like to acknowledge Henry Royce Institute Equipment Grant: EP/P024947/1.

Acknowledgments

We would like to acknowledge Dr Fritsch in providing the facilities for the production of the samples used in this work. This work was supported by the Engineering and Physical Sciences Research Council (Grant Nos. EP/P023088/1 and EP/P026427/1).

ORCID iDs

D A Moseley  <https://orcid.org/0000-0001-7673-0024>

S Speller  <https://orcid.org/0000-0002-6497-5996>

J H Durrell  <https://orcid.org/0000-0003-0712-3102>

References

- [1] Takahashi Y, Naito T, Nakamura T and Takahashi M 2021 Detection of ^1H NMR signal in a trapped magnetic field of a compact tubular MgB_2 superconductor bulk *Supercond. Sci. Technol.* **34** 06LT02
- [2] Gozzelino L *et al* 2020 High magnetic shielding properties of an MgB_2 cup obtained by machining a spark-plasma-sintered bulk cylinder *Supercond. Sci. Technol.* **33** 044018
- [3] Brittles G D, Mousavi T, Grovenor C R M, Aksoy C and Speller S C 2015 Persistent current joints between technological superconductors *Supercond. Sci. Technol.* **28** 093001
- [4] Awaji S, Imai Y, Takahashi K, Okada T, Badel A, Miyazaki H, Hanai S and Ioka S 2019 Field stability analysis of 25 T cryogen-free superconducting magnet and upgrade plans for 30 T system at HFLSM, IMR, Tohoku University *IEEE Trans. Appl. Supercond.* **29** 4300305
- [5] Nakamura T, Itoh Y, Yoshikawa M, Sakai N, Nariki S, Hirabayashi I and Utsumi H 2011 Application of a compact cryogen-free superconducting bulk magnet to NMR *Teion Kogaku* **46** 139–48
- [6] Oka T, Hirayama E, Takahashi Y, Kanai T, Ogawa J, Fukui S, Sato T, Yokoyama K and Nakamura T 2015 Attempt to generate a strong and uniform magnetic field by face-to-face HTS bulk elements in a magnet system *Phys. Proc.* **67** 1005–9
- [7] Nakamura T, Tamada D, Yanagi Y, Itoh Y, Nemoto T, Utumi H and Kose K 2015 Development of a superconducting bulk magnet for NMR and MRI *J. Magn. Reson.* **259** 68–75
- [8] Durrell J H *et al* 2014 A trapped field of 17.6 T in melt-processed, bulk Gd-Ba-Cu-O reinforced with shrink-fit steel *Supercond. Sci. Technol.* **27** 082001
- [9] Namburi D K, Shi Y and Cardwell D A 2021 The processing and properties of bulk (RE)BCO high temperature superconductors: current status and future perspectives *Supercond. Sci. Technol.* **34** 053002
- [10] Berger K, Koblishka M R, Douine B, Noudem J, Bernstein P, Hauet T and Leveque J 2016 High magnetic field generated by bulk MgB_2 prepared by spark plasma sintering *IEEE Trans. Appl. Supercond.* **26** 6801005
- [11] Fuchs G, Häßler W, Nenkov K, Scheiter J, Perner O, Handstein A, Kanai T, Schultz L and Holzapfel B 2013 High trapped fields in bulk MgB_2 prepared by hot-pressing of ball-milled precursor powder *Supercond. Sci. Technol.* **26** 122002
- [12] Rabbers J J, Oomen M P, Bassani E, Ripamonti G and Giunchi G 2010 Magnetic shielding capability of MgB_2 cylinders *Supercond. Sci. Technol.* **23** 125003
- [13] Loudon J C, Yazdi S, Kasama T, Zhigadlo N D and Karpinski J 2015 Measurement of the penetration depth and coherence length of MgB_2 in all directions using transmission electron microscopy *Phys. Rev. B* **91** 054505
- [14] Matthews G A B, Santra S, Ma R, Grovenor C R M, Grant P S and Speller S C 2020 Effect of the sintering temperature on the microstructure and superconducting properties of MgB_2 bulks manufactured by the field assisted sintering technique *Supercond. Sci. Technol.* **33** 054003
- [15] Gozzelino L *et al* 2019 Passive magnetic shielding by machinable MgB_2 bulks: measurements and numerical simulations *Supercond. Sci. Technol.* **32** 034004
- [16] Giunchi G, Raineri S, Wesche R and Bruzzzone P 2004 The voltage–current relations for MgB_2 obtained by reactive liquid infiltration *Physica C* **401** 310–5
- [17] Omori M 2000 Sintering, consolidation, reaction and crystal growth by the spark plasma system (SPS) *Mater. Sci. Eng. A* **287** 183–8
- [18] Naito T, Mochizuki H, Fujishiro H and Teshima H 2016 Trapped magnetic-field properties of prototype for Gd-Ba-Cu-O/MgB_2 hybrid-type superconducting bulk magnet *Supercond. Sci. Technol.* **29** 034005
- [19] Aldica G, Batalu D, Popa S, Ivan I, Nita P, Sakka Y, Vasylykiv O, Miu L, Pasuk I and Badica P 2012 Spark plasma sintering of MgB_2 in the two-temperature route *Physica C* **477** 43–50
- [20] Namba S, Fujishiro H, Naito T, Ainslie M D and Takahashi K 2019 Experimental realization of a hybrid trapped field magnet lens using a GdBaCuO magnetic lens and MgB_2 bulk cylinder *Supercond. Sci. Technol.* **32** 12LT03